



N-n-Butyl-N-methylpyrrolidinium hexafluorophosphate-added electrolyte solutions and membranes for lithium-secondary batteries

Akiko Tsurumaki ^{a,c}, Maria Assunta Navarra ^b, Stefania Panero ^b, Bruno Scrosati ^b, Hiroyuki Ohno ^{a,c,*}

^a Department of Biotechnology, Tokyo University of Agriculture and Technology, 2-24-16 Naka-cho, Koganei, Tokyo 184-8588, Japan

^b Department of Chemistry, The University of Rome "La Sapienza", Piazzale Aldo Moro 5, 00185 Rome, Italy

^c Functional Ionic Liquid Laboratories, Graduate School of Engineering, Tokyo University of Agriculture and Technology, 2-24-16 Naka-cho, Koganei, Tokyo 184-8588, Japan

HIGHLIGHTS

- Safety working range of LiPF₆–EC–DMC was improved after mixing it with ionic liquid.
- The electrolyte solution retained specific charge capacity over 164 mAh g⁻¹ at C/3.
- The electrolyte solution was mixed with PVdF-HFP to form a polymer electrolyte film.
- The ionic conductivity of the film was 4×10^{-4} S cm⁻¹ at room temperature.

ARTICLE INFO

Article history:

Received 3 November 2012

Received in revised form

26 December 2012

Accepted 19 January 2013

Available online 28 January 2013

Keywords:

Ionic liquid

Lithium ion battery

LiPF₆ in EC–DMC

Polymer electrolyte

Thermal stability

Ionic conductivity

ABSTRACT

Polymer electrolytes were prepared using 1 M LiPF₆ in ethylene carbonate–dimethyl carbonate 1:1 wt/wt (LP 30 SelectiLyte™; LP 30 henceforth), *N*-n-butyl-*N*-methylpyrrolidinium hexafluorophosphate ([Py₁₄]PF₆), and poly(vinylidene fluoride-co-hexafluoropropylene) (PVdF-HFP). To determine adequate composition of liquid electrolyte, we investigated the effect of the ratio of [Py₁₄]PF₆ to LP 30, in terms of thermal stability, ionic conductivity and electrochemical stability. The solution, LP 30 with 30 wt% [Py₁₄]PF₆, gave better properties compared to pure LP 30 and other mixtures examined in this study. Then this was used for galvanostatic charge–discharge tests of a lithium cell. The cell, with the chosen electrolyte solution, demonstrated reversible capacity reaching the theoretical values, when Li metal was combined with LiFePO₄ or Li₄Ti₅O₁₂ electrode. A polymer membrane was prepared by combining the chosen solution with PVdF-HFP matrix. The ionic conductivity of this membrane was 4×10^{-4} S cm⁻¹ at room temperature. Furthermore, the polymer electrolyte displayed reasonable thermal stability, reflecting the properties of [Py₁₄]PF₆ in improving the performance of the polymer electrolyte.

© 2013 Elsevier B.V. All rights reserved.

1. Introduction

Lithium ion batteries are vital components of portable devices such as mobile phones and laptop computers, because of their high energy density [1,2]. With the growth of the market in portables and advances in cell performance, there is a strong request to improve credibility and thermal- and electrochemical-stabilities.

The electrolyte is the critical component involved in balancing energy and safety specifications. LiPF₆ is acknowledged as one of potential salts for lithium ion batteries because it has a unique set of

properties that include sufficient ionic conductivity and negligible reactivity toward aluminum current collectors [3,4]. The chemical stability and dissociation rate of LiPF₆ have been improved by adding a high dielectric carbonate solvent [5], and 1 M LiPF₆ in ethylene carbonate (EC)–dimethyl carbonate (DMC) 1:1 wt/wt mixture (LP 30 SelectiLyte™; LP 30 henceforth) has been commercialized as a conventional electrolyte solution for lithium ion batteries. The presence of EC also assists the formation of the solid electrolyte interface (SEI), which protects and enhances ion transfer on the graphite surface. However, the use of LP 30 presents safety hazards because of the volatility of carbonate-components, the limited temperature range for safe ion conduction, and fear of leakage of the solution.

Various attempts have been made to overcome these problems. An approach which reduces flammability is the replacement or the hybridization of volatile carbonates with ionic liquids (ILs). ILs are molten salts at ambient temperature and some of these have been

* Corresponding author. Department of Biotechnology, Tokyo University of Agriculture and Technology, 2-24-16 Naka-cho, Koganei, Tokyo 184-8588, Japan. Tel./fax: +81 42 388 7024.

E-mail addresses: [\(A. Tsurumaki\)](mailto:50012831205@st.tuat.ac.jp), [\(M.A. Navarra\)](mailto:mariassunta.navarra@uniroma1.it), [\(S. Panero\)](mailto:stefania.panero@uniroma1.it), [\(B. Scrosati\)](mailto:bruno.scrosati@uniroma1.it), [\(H. Ohno\)](mailto:ohnoh@cc.tuat.ac.jp).

studied as potential electrolyte media in batteries, because they have negligible low vapor pressure, non-flammability, and desired ionic conductivity over a wide range of temperatures [6]. Many materials have been studied with Li salt-doped ILs, which give very attractive electrolytes having high ionic conductivity, non-flammability, and excellent charge–discharge efficiency and capability with different types of anode and cathode. An imidazolium-based IL (ex. 1-ethyl-3-methylimidazolium bis(trifluoromethanesulfonyl)imide; [C₂mim][TFSI]) has been studied because of its low viscosity and relatively high ionic conductivity. However, imidazolium-based ILs are not suitable for lithium batteries because of their cathodic limit (1 V vs. Li⁺/Li) arising from acidic protons on the imidazolium ring [7]. Therefore, the challenge is to increase cathodic stability by using aliphatic cations such as pyrrolidinium [8,9], quaternary phosphonium [10], and quaternary ammonium [11]. Systems based on *N*-n-propyl-*N*-methylpyrrolidinium bis(fluorosulfonyl)imide ([Py₁₃][FSI]) mixed with LiTFSI displayed an excellent reversible capacity of ~144 mAh g⁻¹ at C/2 and negligible capacity fade over several hundred cycles with lithium iron phosphate [12]. Further improvement is still on going, as the addition of Li salts to an IL usually leads to an increase in viscosity due to enhanced ion–ion interactions [13]. The formation of hybrid electrolytes based on mixtures of ILs and standard carbonate solvents is beneficial to the viscosity, formation of SEI, and relative cycle performance while retaining less-flammability [14–16]. Xiang et al. reported a LiTFSI doped piperidinium-based IL with discharge capacities of 140 and 100 mAh g⁻¹ with lithium cobalt oxide, with and without carbonate solvents respectively [17]. Moreover, the idea of using IL-Li salt mixtures or their further mixture with alkyl carbonate solutions in order to form a solid-state polymer electrolyte has been successfully demonstrated, achieving improved safety and stability. Focusing on ionic conductivity, Appetecchi et al. demonstrated IL-doped polyether-based polymer electrolytes with ionic conductivity exceeding 10⁻⁴ S cm⁻¹ at 20 °C [18] and their enhanced performance in terms of specific capacity, energy cycle life, and coulombic efficiency [19]. In considering stability, fluorinated polymer, especially a copolymer of vinylidene fluoride with hexafluoropropylene, is a remarkable matrix enhancing ionic conductivity; it corresponds to a polyether system, having mechanical and chemical stability [20,21].

We present here a new class of IL-added LP 30 solutions and membranes as electrolytes for lithium-secondary batteries, using ILs composed of pyrrolidinium cations and PF₆ anions.

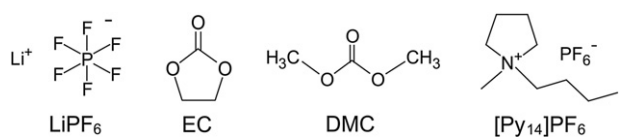
2. Experimental section

2.1. Materials

Battery grade electrolytes, namely LP 30 (from Merck), DMC (from Sigma–Aldrich Co.) were stored in an Ar-filled glove box. DMC solvent was purified with zeolite before use. Poly(vinylidene fluoride-co-hexafluoropropylene), Kynar Flex® 2801 (PVdF-HFP henceforth, from Atofina) and *N*-n-butyl-*N*-methylpyrrolidinium hexafluorophosphate ([Py₁₄]PF₆, from Solvionic) were dried in a vacuum at 120 °C for 12 h prior to use.

2.2. Preparation of the electrolyte solutions and membranes

Scheme 1 shows the chemical structure of LiPF₆, EC, DMC and [Py₁₄]PF₆. A series of solutions was prepared by varying the [Py₁₄]PF₆ content in LP 30 from 5 to 30 wt%. **Table 1** shows the compositions and acronyms of the resulting solutions. The water content of all solutions prepared was less than 20 ppm according to a standard Karl Fischer titration method, 831 kF Coulometer (from Metrohm). All procedures were carried out in an Ar-filled glove box.



Scheme 1. Chemical structure of electrolyte components used in this study.

PVdF-HFP-based polymer membranes were prepared by a solution casting procedure. We selected DMC as a diluting solvent, since EC–DMC cosolvent is the solvent of LP 30, and DMC was evaporated at lower temperature than EC in the cosolvent [22]. Initially, 0.3 g of PVdF-HFP was dissolved in 5.0 g of DMC. Sol-30 was selected as the electrolyte solution, and 0.7 g of it was added to the PVdF-HFP–DMC solution. The resulting solution was stirred vigorously at room temperature overnight, then for 10 min at 70 °C. The mixture was cast on a 5 cm diameter Petri dish at 70 °C. To evaporate the DMC, the Petri dish was heated for 1 h at 70 °C and quenched to room temperature for 1 h. The heating-quenching procedures were repeated four times, and additional shorter cycles until a weight loss of ca. 5.0 g had occurred, corresponding to removal of the DMC solvent. The polymer membrane we obtained had thickness of 200 ± 10 µm and was stored in immersion in the electrolyte solution (i.e., sol-30) prior to use. All procedures and handling of materials were carried out in an Ar-filled glove box.

2.3. Thermal properties

We have carried out differential scanning calorimetry (DSC) measurements using a DSC 821 (from Mettler-Toledo) equipped with a liquid nitrogen cooling system. The sample pans were sealed in an Ar-filled glove box and measurements were carried out in ambient atmosphere. The samples were cooled to -95 °C with a rate of -10 °C min⁻¹ and held for 7 min, then DSC scans were taken from -90 to 90 °C with a scan rate of 3 °C min⁻¹. Thermogravimetric analyses (TGA) were carried out using a TGA/SDTA 851 (from Mettler-Toledo) in ambient atmosphere from room temperature to 600 °C with a scan rate of 5 °C min⁻¹.

2.4. Electrochemical properties

Ionic conductivity was measured by electrochemical impedance spectroscopy, using a frequency response analyzer, FRA 1260 (from Solatron). A cell consisted of two platinum electrodes immersed in the electrolyte solution, with a nominal cell constant of 0.98 cm⁻¹. In the case of the polymer electrolyte, cells were fabricated by sandwiching a disk of a membrane with two stainless steel electrodes. The cells were tightly sealed in an Ar-filled glove box and measurements were carried out in ambient atmosphere. A signal of amplitude 5 mV was applied to the cell in the frequency range of 100 kHz–1 Hz. Conductivity was measured every 5 °C from -30 to 30 °C after equilibration for ca. 8 h at each temperature.

The electrochemical stability window was determined by linear sweep voltammetry and cyclic voltammetry, using a multi-channel potentiostat/galvanostat/impedance analyzer, VersaSTAT MC (from Princeton Applied Research). Cells were fabricated by sandwiching three disks of glass fiber separators (Whatman™ GF/A

Table 1
Composition of the solutions used in this study.

Sample name	Component ratio/wt%	
	LP 30	[Py ₁₄]PF ₆
sol-5	95	5
sol-20	80	20
sol-30	70	30

separator) with two electrodes. Super P carbon-coated Al or Cu plate was used as the working electrode, and Li foil was used as the counter electrode. The cells were tightly sealed in an Ar-filled glove box and measurements were carried out in ambient atmosphere. Voltammetry was performed with a scan rate of 0.2 mV s^{-1} .

The interfacial resistance between electrolyte and Li metal electrode was determined by impedance spectroscopy analysis, using a FRA 1260. We used cells formed by symmetrical Li metal electrodes and three disks of electrolyte-soaked Whatman™ GF/A separators between them, and applied a 5 mV amplitude signal to the cell in the frequency range of 150 kHz–10 Hz. Impedance measurement was carried out every day for nearly two months, and spectrum was fitted according to an equivalent circuit using a ZSimp-Win 3.21 program. All procedures were carried out in an Ar atmosphere at room temperature.

Galvanostatic charge–discharge behavior was tested using a Series 4000 battery test system (from Maccor) as the driving and controlling instrument. Cells were fabricated by sandwiching two disks of electrolyte-soaked Whatman™ GF/A separators with Li metal and $\text{Li}_4\text{Ti}_5\text{O}_{12}$ (LTO) or LiFePO_4 (LFP). The cells were tightly sealed in an Ar-filled glove box and measurements were carried out in ambient atmosphere. The cell was cycled galvanostatically at C/5 (1C current is equivalent to 0.473 mA cm^{-2}) using LTO, and at C/3 (1C current is equivalent to 0.650 mA cm^{-2}) using LFP.

3. Results and discussion

3.1. Thermal properties and ionic conductivity of the electrolyte solutions

To investigate the effect of adding ILs, we have analyzed thermal properties and ionic conductivities over a wide range of temperatures. Fig. 1 shows the DSC traces of $[\text{Py}_{14}]PF_6$, LP 30, and their hybrid electrolytes. With $[\text{Py}_{14}]PF_6$, a main endothermic transition is observed at 86°C , corresponding to the expected melting behavior of the IL. This phase transition, together with two minor features at around -80 and 46°C , is not observed after mixing IL with LP 30, confirming the existence of strong ionic and molecular interactions among components of the resulting solutions. New peaks are observed below 0°C in the hybrid electrolytes, deriving from the thermal transitions that typically relate to LP 30 and are affected in our experiment by the IL component. With LP 30 and its mixture with IL, two exothermic peaks are observed, corresponding

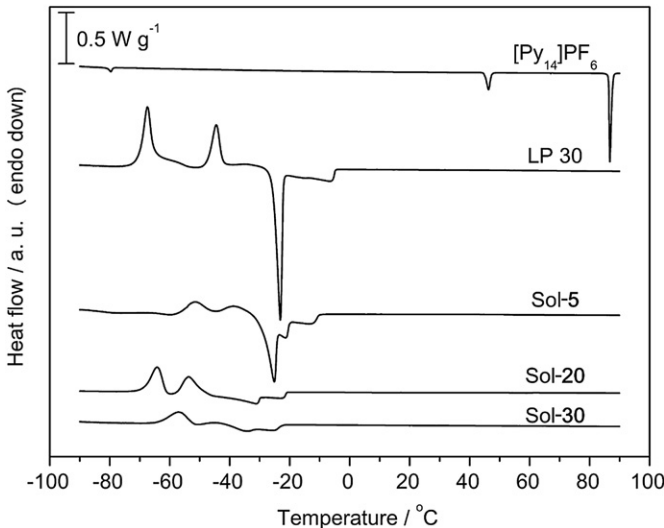


Fig. 1. DSC curves for $[\text{Py}_{14}]PF_6$, LP 30, and sol-5, sol-20, and sol-30.

to solid–solid transition or cold crystallization of LP 30 [23]. Also, a typical endothermic response appears around -23°C and is due to the main melting of LP 30. This melting feature is followed by obscure endothermic phenomenon around -5°C , which is often observed in such composite electrolytes [22], and can be ascribed to the heterogeneity of the system, including potential salt segregation/dissolution. All these features are strongly smoothed by the addition of IL and the temperatures of both endothermic phenomena shift downward.

Fig. 2 shows the Arrhenius plots of ionic conductivity versus temperature from -30 to 30°C . The ion conduction of LP 30 is known to be suppressed at temperatures below its crystallization point [23]. The ionic conductivity of crystallized sol-5 and sol-20 increases dramatically near the melting temperatures. The ionic conductivity of sol-30 exhibits only a smooth change, and the Arrhenius plots obey a Vogel–Fulcher–Tammann behavior. This may be because $[\text{Py}_{14}]PF_6$ has a plastic crystal phase, as reported previously [24], and the adequate addition of $[\text{Py}_{14}]PF_6$ causes hybrid electrolytes to become amorphous at low temperature. As a result, the desired ionic conductivity ($>10^{-3} \text{ S cm}^{-1}$) prevails even at -27°C with sol-30, and its ionic conductivity is 16 times greater than that of sol-5, containing 5 wt% IL. We confirm that the addition of $[\text{Py}_{14}]PF_6$ suppresses the crystallization of LP 30, and allows ion conduction sufficient enough for applications over a wide temperature range.

3.2. Electrochemical stability and cell performance of the electrolyte solutions

With a view to applying LP 30– $[\text{Py}_{14}]PF_6$ hybrid electrolytes in lithium batteries, electrochemical stability was analyzed in terms of the electrochemical potential window and interfacial resistance with Li metal; an effective component ratio of the electrolytes was determined from among those investigated. Fig. 3 shows the electrochemical stability window for the electrolytes. The linear anodic scan in Fig. 3A shows that the onset of small currents occurs

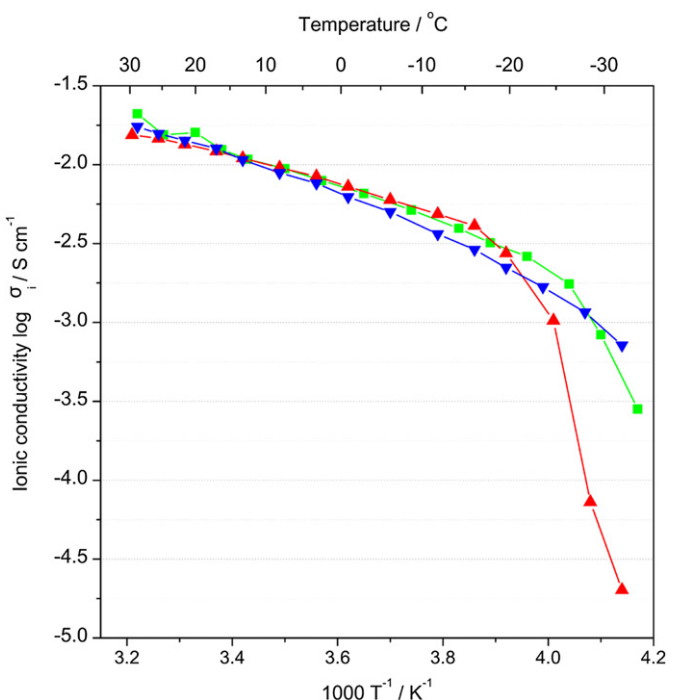


Fig. 2. Arrhenius plots of ionic conductivity versus temperature for sol-5 (▲), sol-20 (■), and sol-30 (▼).

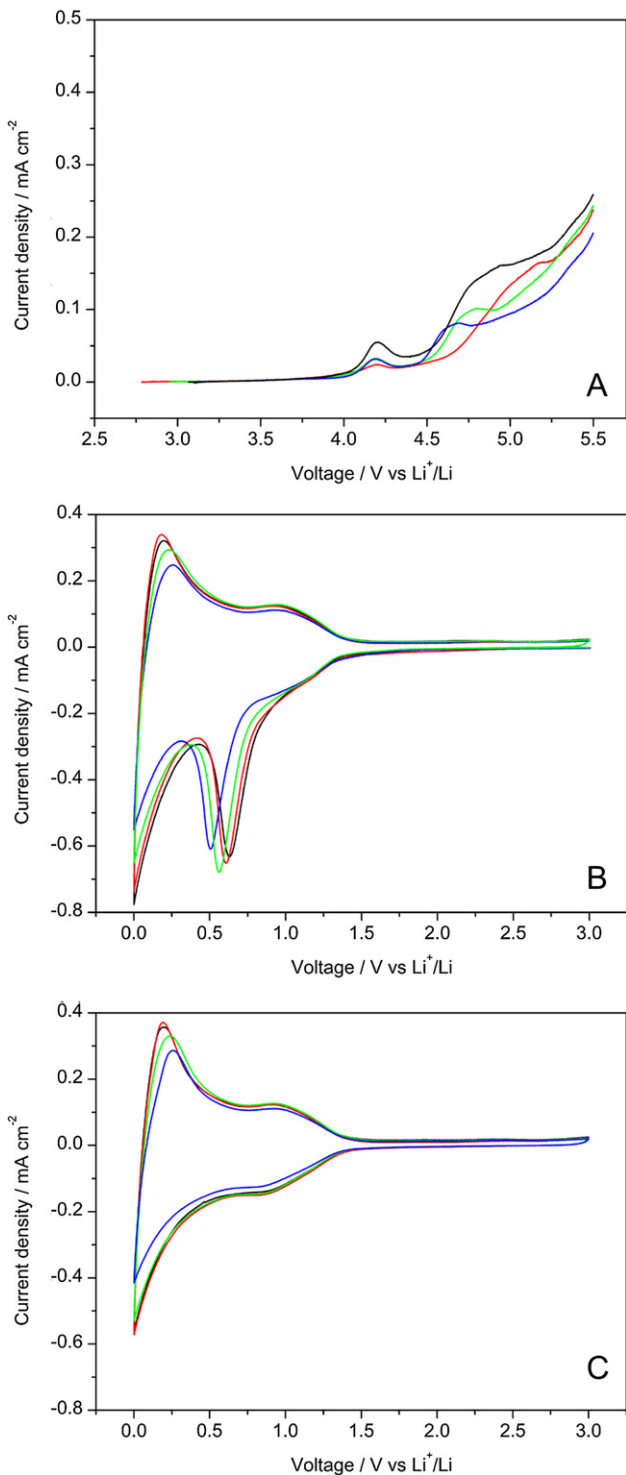


Fig. 3. Electrochemical stability window of LP 30 (black), sol-5 (red), sol-20 (green), and sol-30 (blue). (A) Anodic scan of linear sweep voltammetry with Super P carbon-coated Al working electrode, (B) first cycle, and (C) second cycle of cyclic voltammetry with Super P carbon-coated Cu working electrode. (For interpretation of the references to color in this figure legend, the reader is referred to the web version of this article.)

at around 4 V, after which they settle down and remain less than 0.1 mA cm^{-2} up to 4.6 V for the electrolytes containing ILs. Anodic stability is slightly affected by the presence of the IL. By taking the identical structure of the LP 30 and IL anions into account, the differences observed among the various solutions toward oxidation can be related to differing mobility of the electrolyte components.

Fig. 3B shows the cyclic voltammetry of the electrolyte solution, and all cathodic scans show three clear stages. The first current drift appears below 1.5 V, followed by a clear peak around 0.5 V and another current response at ca. 0 V. The peak at around 0.5 V shifts to the lower potential side upon adding IL, and disappears in the second cathodic scans (see Fig. 3C). It relates to an irreversible initial decomposition of the electrolyte components, which lead to the formation of a protective passivation layer on the electrode surface. Current responses below 1.5 V and at ca. 0 V are almost reproducible after the second cycle, and are related to typical lithium insertion into carbon; this is confirmed by the presence of the corresponding oxidation features in the reverse scan. The electrochemical stability window is expanded, by the addition of the IL, as a result of specific ionic and/or dipole interactions.

Fig. 4 shows the interfacial resistance change over a 2 month period. To analyze the interfacial resistance, cells formed by sandwiching each of the four electrolytes investigated with two Li metal electrodes are prepared, and their impedance is measured (see Figure S1 in the Supplementary information). In Fig. 4, each point is derived by evaluation of the amplitude of a semicircle from the impedance spectrum in the Nyquist plot with increasing times of storage. Throughout the experiments, measurements were carried out at room temperature. Accordingly, the changes in the same manner should be attributed to the different daily temperature. In the first period, the interfacial resistances increase as a result of the formation of a SEI film. In the mid-term, around 15 days, the interfacial resistances are found to decrease slightly. This may be due to the change in the morphology of SEI. For LP 30, sol-5, and sol-20, interfacial resistance begins to increase again and reaches a virtually constant value after 30 days. Sol-30 exhibits a stable and well controlled interfacial behavior with constant resistances from 15 days onward. It is well known that the formation of SEI is affected by the environment of the electrolytes, involving such factors as the salt concentration, electrolyte composition, and salt solvation [25–27]. For the case of sol-30, a larger number of [Py₁₄]PF₆ species exists in LP 30 electrolyte than that for other solutions investigated, probably resulting in qualitatively different and more effective solvation of carbonate compounds to ions. Addition of an adequate amount of [Py₁₄]PF₆ improves the properties of the composite electrolyte, leading to enhanced low-temperature conductivity and electrochemical stability. Based on these results, sol-30 is the most suitable composition of those investigated.

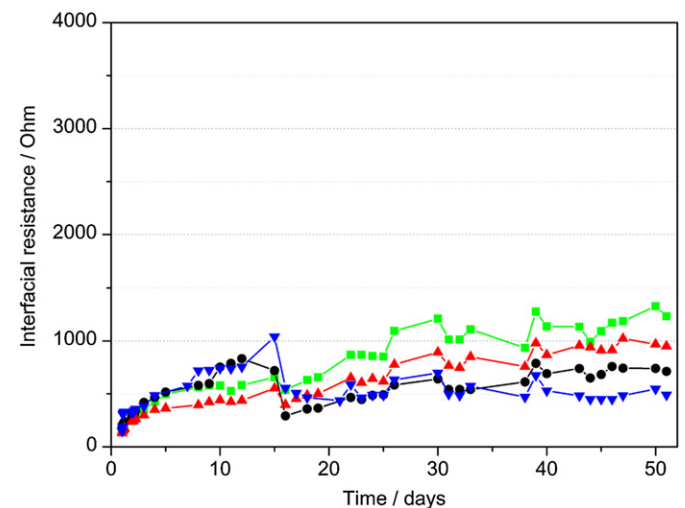


Fig. 4. Resistance at the electrolyte/Li metal interface. ●: LP 30, ▲: sol-5, ■: sol-20, and ▽: sol-30.

Fig. 5 shows the charge–discharge profiles during the cycle for the cell comprising sol-**30** sandwiched with Li metal and LTO or LFP, respectively. A fairly high coulombic efficiency is observed in both cells. For the cell with LTO (**Fig. 5A**), the specific capacity reaches 168 mAh g^{-1} at C/5, which is 96% of the theoretical value. Although there is a slight decrease in capacity with increasing cycle number, the reversible capacity retains over 92% of the theoretical value. The cell with LFP gives flat voltage profiles (**Fig. 5B**) and high specific capacity of at least 164 mAh g^{-1} at C/3, which is 96% of the theoretical value, from 1 to 10 cycles. These data all show that sol-**30** (i.e., LP 30 with 30 wt% $[\text{Py}_{14}] \text{PF}_6$) is confirmed to be effective as electrolyte solution for lithium batteries.

3.3. Properties of the polymer electrolyte membrane

We have found that sol-**30** is an excellent electrolyte solution suitable for deployment the preparation of polymer electrolytes. We have successfully prepared PVdF-HFP based membranes. In this work, acetonitrile, which is typically used as a solution for polymer electrolyte mixture, is replaced with the volatile DMC (a component of LP 30), which is expected to act as both a dispersing and

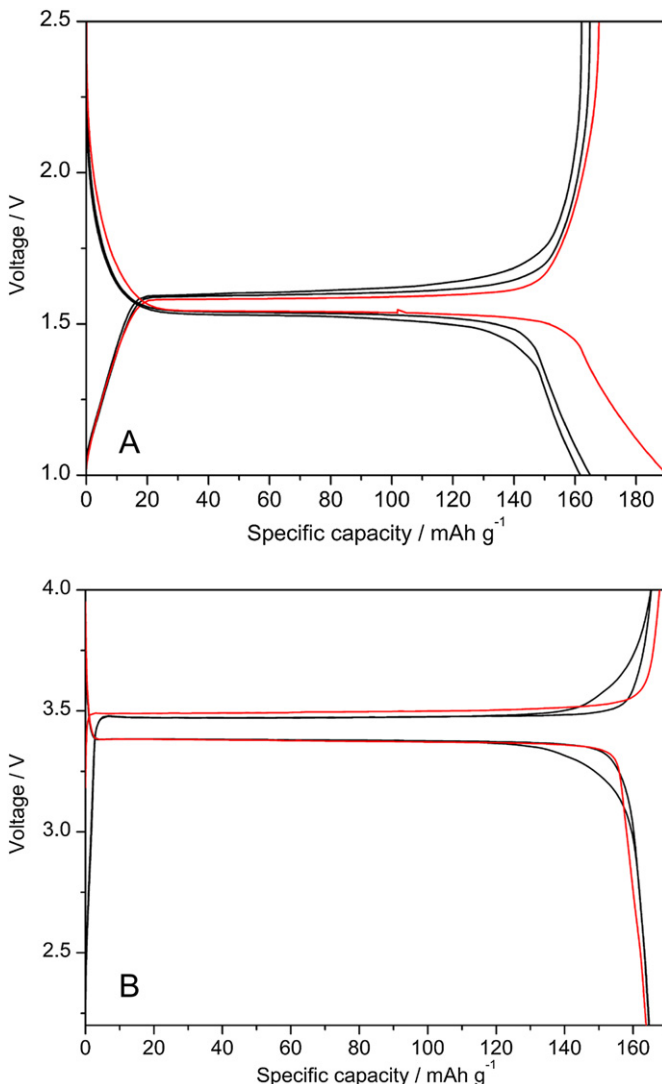


Fig. 5. Charge–discharge behavior of (A) Li/sol-**30**/LTO and (B) Li/sol-**30**/LFP at C/5 and C/3 rate, respectively (1st cycle in red, 5th and 10th cycles in black). (For interpretation of the references to color in this figure legend, the reader is referred to the web version of this article.)



Fig. 6. Photo of a membrane composed of sol-**30** and PVdF-HFP before storing it in sol-**30**.

plasticizing agent. This allows us to manage the removal of the solvent during the preparation of the membrane (see Experimental section). The polymer electrolyte membranes are prepared with the method reported previously by us [28]. **Fig. 6** shows a picture of the membrane prepared in this work. The resulting polymer electrolytes are immersed in sol-**30** so as store the membrane without risk of segregation or lithium salt decomposition.

TG analysis, shown in **Fig. 7**, provides information on both composition and thermal properties of the polymer electrolyte after immersing it in sol-**30**. Weight loss up to 150°C is due to the removal of the carbonate-based electrolyte components; the weight loss above 300°C is due to the decomposition of $[\text{Py}_{14}] \text{PF}_6$, and the third sequence of weight loss is related to the decomposition of the PVdF-HFP matrix. The leftover weight at the end of the temperature scan can be assigned to carbonaceous residuals. **Fig. 7** shows that about 30 wt% of IL remained in the membrane, suggesting flame retardation. According to previous work, the concentration of IL we used in sol-**30** is high enough to control or strongly reduce the flammability of the resulting electrolyte [29–31].

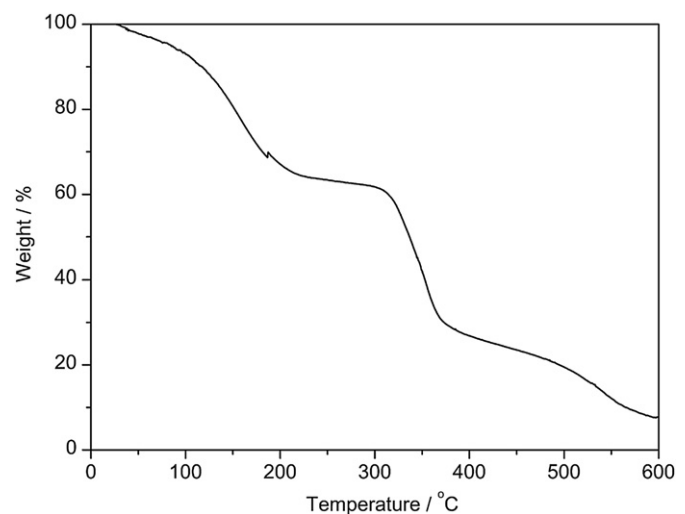


Fig. 7. TGA chart of the polymer electrolyte composed of sol-**30** and PVdF-HFP after immersing in sol-**30**.

The membrane prepared here has conductivity 4×10^{-4} S cm $^{-1}$, at room temperature, suggesting suitability for polymer electrolytes. Full electrochemical characterization of such membranes, and their transport properties, is under way.

4. Conclusion

We have studied the effect of adding [Py₁₄]PF₆ on the properties of LP 30, and proposed an optimized composition so as to yield a polymer electrolyte having superior performance. The solution formed by LP 30 with 30 wt% of [Py₁₄]PF₆, named sol-**30**, had better thermal and electrochemical properties than the liquid electrolyte solutions investigated here. Lithium-metal cells, equipped with this sol-**30**, had a capacity comparable to that of most conventional, benchmark electrolyte-based cells. Additionally, sol-**30** was combined with PVdF-HFP matrix to form polymer electrolyte membranes. The polymer electrolyte membrane had practical conductivity ($>10^{-4}$ S cm $^{-1}$) and desirable thermal stability.

Acknowledgments

This work has been performed as part of a collaborative research agreement between the Department of Chemistry, University of Rome “La Sapienza” and the Department of Biotechnology of Tokyo University of Agriculture and Technology. A.T. acknowledges financial support from the JSPS International Training Program (ITP). H.O. acknowledges financial support from a Grant-in-Aid for Scientific Research from the Japan Society for the Promotion of Science (No. 21225007).

Appendix A. Supplementary data

Supplementary data related to this article can be found at <http://dx.doi.org/10.1016/j.jpowsour.2013.01.131>.

References

- [1] B. Scrosati, J. Garche, *J. Power Sources* 195 (2010) 2419–2430.
- [2] P.G. Bruce, B. Scrosati, J.-M. Tarascon, *Angew. Chem. Int. Ed.* 47 (2008) 2930–2946.
- [3] M. Dahbi, F. Ghamous, F. Tran-Van, D. Lemordant, M. Anouti, *J. Power Sources* 196 (2011) 9743–9750.
- [4] M. Morita, T. Shibata, N. Yoshimoto, M. Ishikawa, *Electrochim. Acta* 47 (2002) 2787–2793.
- [5] T. Kawamura, S. Okada, J. Yamaki, *J. Power Sources* 156 (2006) 547–554.
- [6] M. Armand, F. Endres, D.R. MacFarlane, H. Ohno, B. Scrosati, *Nat. Mater.* 8 (2009) 621–629.
- [7] B. Garcia, S. Lavallée, G. Perron, C. Michot, M. Armand, *Electrochim. Acta* 49 (2004) 4583–4588.
- [8] J. Hassoun, A. Fericola, M.A. Navarra, S. Panero, B. Scrosati, *J. Power Sources* 195 (2010) 574–579.
- [9] P. Reale, A. Fericola, B. Scrosati, *J. Power Sources* 194 (2009) 182–189.
- [10] K. Tsunashima, A. Kawabata, M. Matsumiya, S. Kodama, R. Enomoto, M. Sugiyama, Y. Kunugi, *Electrochim. Commun.* 13 (2011) 178–181.
- [11] H.H. Zheng, K. Jiang, T. Abe, Z. Ogumi, *Carbon* 44 (2006) 203–210.
- [12] A.P. Lewandowski, A.F. Hollenkamp, S.W. Donne, A.S. Best, *J. Power Sources* 195 (2010) 2029–2035.
- [13] A. Martinelli, A. Matic, P. Jacobsson, L. Börjesson, A. Fericola, B. Scrosati, *J. Phys. Chem. B* 113 (2009) 11247–11251.
- [14] G.H. Lane, A.S. Best, D.R. MacFarlane, M. Forsyth, P.M. Bayley, A.F. Hollenkamp, *Electrochim. Acta* 55 (2010) 8947–8952.
- [15] L. Larush, V. Borgel, E. Markevich, O. Haik, E. Zinigrad, D. Aurbach, G. Semrau, M. Schmidt, *J. Power Sources* 189 (2009) 217–223.
- [16] A. Lewandowski, A. Świderska-Mocek, *J. Power Sources* 194 (2009) 601–609.
- [17] H.F. Xiang, B. Yin, H. Wang, H.W. Lin, X.W. Ge, S. Xie, C.H. Chen, *Electrochim. Acta* 55 (2010) 5204–5209.
- [18] G.B. Appetecchi, C.T. Kim, M. Montanino, F. Alessandrini, S. Passerini, *J. Power Sources* 196 (2011) 6703–6709.
- [19] G.T. Kim, S.S. Jeong, M.Z. Xue, A. Balducci, M. Winter, S. Passerini, F. Alessandrini, G.B. Appetecchi, *J. Power Sources* 199 (2012) 239–246.
- [20] H. Ye, J. Huang, J.J. Xu, A. Khalfan, S.G. Greenbaum, *J. Electrochem. Soc.* 154 (2007) A1048–A1057.
- [21] A. Fericola, F.C. Weise, S.G. Greenbaum, J. Kagimoto, B. Scrosati, A. Soletti, *J. Electrochem. Soc.* 156 (2009) A514–A520.
- [22] A. Ponrouch, E. Marchante, M. County, J.-M. Tarascon, M.R. Palacín, *Energy Environ. Sci.* 5 (2012) 8572–8583.
- [23] P.E. Stallworth, J.J. Fontanella, M.C. Wintersgill, C.D. Scheidler, J.J. Immel, S.G. Greenbaum, A.S. Gozdz, *J. Power Sources* 81–82 (1999) 739–747.
- [24] J. Golding, N. Hamid, D.R. MacFarlane, M. Forsyth, C. Forsyth, C. Collins, J. Huang, *Chem. Mater.* 13 (2001) 558–564.
- [25] D. Fauteux, *J. Electrochem. Soc.* 135 (1988) 2231–2237.
- [26] S.K. Jeong, M. Inaba, Y. Iriyama, T. Abe, Z. Ogumi, *Electrochim. Acta* 47 (2002) 1975–1982.
- [27] R. Naejus, R. Coudert, P. Willmann, D. Lemordant, *Electrochim. Acta* 43 (1998) 275–284.
- [28] M.A. Navarra, J. Manzi, L. Lombardo, S. Panero, B. Scrosati, *ChemSusChem* 4 (2011) 125–130.
- [29] A. Guerfi, M. Dontigny, P. Charest, M. Petitclerc, M. Lagacé, A. Vijh, K. Zaghib, *J. Power Sources* 195 (2010) 845–852.
- [30] C. Arbiziani, G. Gabrielli, M. Mastragostino, *J. Power Sources* 196 (2011) 4801–4805.
- [31] L. Lombardo, S. Brutti, M.A. Navarra, S. Panero, P. Reale, *J. Power Sources* 227 (2013) 8–14.